National Physical Laboratory

NPL REPORT MAT 94

INFLUENCE OF H_2S ON THE LOCALISED CORROSION OF 316L STAINLESS STEEL: PART 2 – ELECTROCHEMICAL TESTING

JAMES HESKETH, EDMUND J.F. DICKINSON, ALAN TURNBULL AND GARETH HINDS

MAY 2020

INFLUENCE OF H_2S ON THE LOCALISED CORROSION OF 316L STAINLESS STEEL: PART 2 – ELECTROCHEMICAL TESTING

James Hesketh, Edmund J.F. Dickinson, Alan Turnbull and Gareth Hinds

Department of Electromagnetic and Electrochemical Technologies

SUMMARY

This report describes the second part of a two-part study to elucidate the mechanism by which H_2S leads to pitting of stainless-steel in environments representative of upstream oil and gas applications. In this part, a series of electrochemical tests was performed to measure the impact of H_2S on the anodic and cathodic reaction kinetics of 316L stainless steel in H_2S/CO_2 containing brines. The electrochemical testing included cyclic polarisation, cathodic polarisation and artificial pit measurements.

The passivity of the film appeared to be reduced with increasing H_2S concentration but the trend depended on the pH/buffering combination and was not fully consistent. The repassivation potentials derived from anodic polarisation tests with different partial pressures of H_2S in simulated oilfield environments did not reflect the pitting behaviour observed in coupon tests, suggesting that the methodology used for the cyclic polarisation tests was overly severe.

Cathodic polarisation tests in 0.1 bar H_2S supported other published work, which suggested that the role of H_2S in solution in relation to cathodic reduction was that of a weak buffer rather than being itself cathodically reduced. This proposition was not consistent with repeatable data obtained at 0.01 bar H_2S, where a clearly discerned increase in cathodic current density near the open circuit potential (OCP) attributable to the presence of H_2S was apparent, together with a shift in OCP to less negative potentials. For this case, pre-exposure also led to an enhancement of the cathodic current density. Direct reduction of H_2S with a catalytic effect associated with the complex sulphide/oxide film would explain the observations at 0.01 bar H_2S. However, reduction of a metal sulphide film formed during pre-exposure cannot be excluded. The absence of any increased current density at 0.1 bar H_2S does not align with either suggestion and highlights the complexity in interpreting measurements in H_2S environments.

The anodic current density in the artificial pit was relatively high under coupling conditions, which would imply rapid pit growth. This would suggest that most of the pits observed ex situ following materials qualification testing have already stopped growing significantly.

ISSN 1754-2979

https://doi.org/10.47120/npl.MAT94

National Physical Laboratory
Hampton Road, Teddington, Middlesex, TW11 0LW

Approved on behalf of NPL by
Dr Fernando Castro, Head of Science, Department of Electromagnetic & Electrochemical Technologies

CONTENTS

1 INTRODUCTION

Stress corrosion cracking of 316L stainless steel (SS) in oilfield environments containing H_2S often initiates at corrosion pits[1]. However, understanding of the primary factors controlling pit development is not well developed. Experimental measurements of pitting behaviour in well-defined laboratory coupon testing were undertaken to elucidate the impact of H_2S concentration. The investigation highlighted the importance of metal sulphide precipitation and local pH in the pit in determining the extent to which pits would propagate. These results and associated discussion are reported in Part 1 of this report[2]. In addition to these coupon tests, a series of electrochemical measurements were undertaken to provide complementary insight and to aid interpretation of the coupon measurements. The results of this testing are reported here.

2 MATERIAL CHARACTERISATION

All testing was performed on test specimens prepared from the mid-thickness of a 15 mm thick UNS S31603 (316L SS) plate (NPL material reference code – AFUQ), whose composition is shown in Table 1, and is identical to that adopted in the coupon testing. The alloy has an equiaxed austenitic grain structure with delta ferrite bands orientated with the rolling plane as shown in Figure 1. Identification of δ-ferrite was confirmed using scanning electron microscopy (SEM) and electron backscatter diffraction (EBSD), as shown in Figure 2.

Table 1: Composition of the 316L SS tested in this work (mass%) (AFUQ).

C	Si	Mn	P	S	Cr	Ni	Mo	N	Cu	Fe
0.015	0.43	1.28	0.030	0.002	16.75	10.07	2.05	0.043	0.41	Bal.

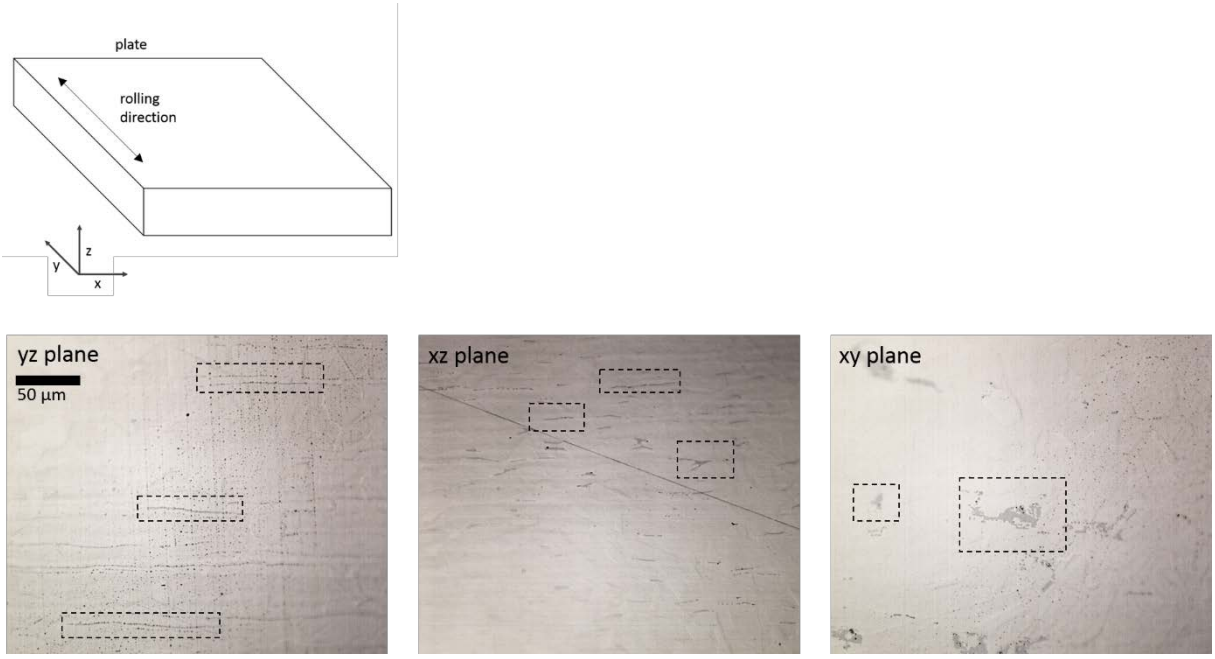

Figure 1: Optical micrograph showing 316L SS microstructure with bands of δ-ferrite highlighted.

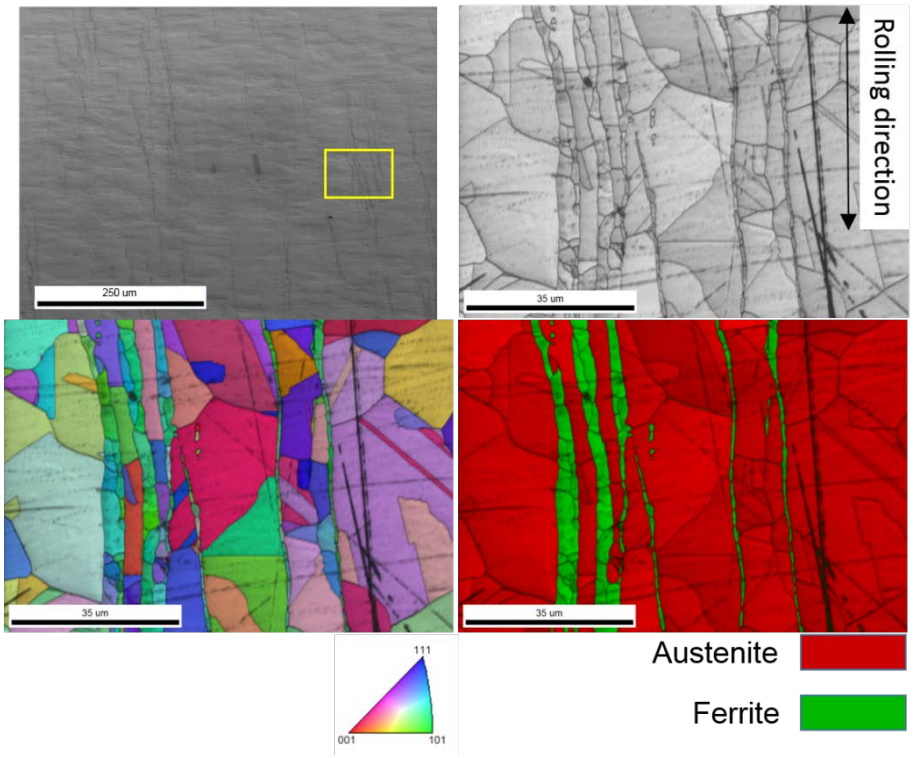

Figure 2: Electron micrographs showing microstructure of 316L SS used in this work. Electron backscatter diffraction (EBSD) has been used to show grain orientation (bottom left) and phase (bottom right).

3 EXPERIMENTAL

3.1 PITTING AND REPASSIVATION

3.1.1 Outline

A series of cyclic polarisation tests was performed to establish the influence of H_2S partial pressure on the pitting and repassivation characteristics of 316L SS in representative oilfield brines. These experiments were intended to show how H_2S concentration influences the corrosion potential, pitting potential and repassivation potential of 316L SS in environments that are close to and beyond its limit regarding resistance to SCC. The tests are very quick to run in comparison to immersion tests and offer a convenient way of assessing the corrosivity of an environment with respect to a given alloy. However, pits that are generated under anodic polarisation may differ significantly, in both morphology and local chemistry, from pits that form under open circuit conditions, such as those produced on pitting coupon specimens.

Additional tests were also performed to try and decouple the effect on the electrochemistry of H_2S in solution and its parallel role in modifying the composition and stability of the passive film. This was explored by pre-exposing specimens to H_2S-containing solutions before then polarising in the presence of CO_2 but with no H_2S present in the bulk solution.

3.1.2 Pitting and repassivation specimens

Pitting and repassivation specimens consisted of a 316L SS rod 0.7-0.8 cm in diameter, 40 cm in length containing a 10 cm long PEEK sheath at one end to allow electrical isolation from the metallic compression fitting seal. The specimens were machined and ground (grinding wheel) to give an average surface roughness Ra < 0.2 μm. The design of these specimens allows local cooling to be administered to the bottom third of the exposed metallic section (~ 10 cm), which is held outside the

autoclave whilst the top two-thirds (~ 20 cm) are housed within the autoclave (see Figure 3); this prevents crevice corrosion from taking place at the PEEK seal. This results in a temperature differential along the length of the specimen (see Figure 4), meaning that during anodic polarisation in H_2S, pitting only takes place towards the hotter top-end of the specimen. Therefore, the current density along the specimen is not uniform. It is assumed that all the current is associated with the 20 cm section that is at approximately constant temperature (Figure 4). In practice, this only gives a very slight over-estimation of the true current density as the portion of the specimen that is outside of the autoclave remains fully passive.

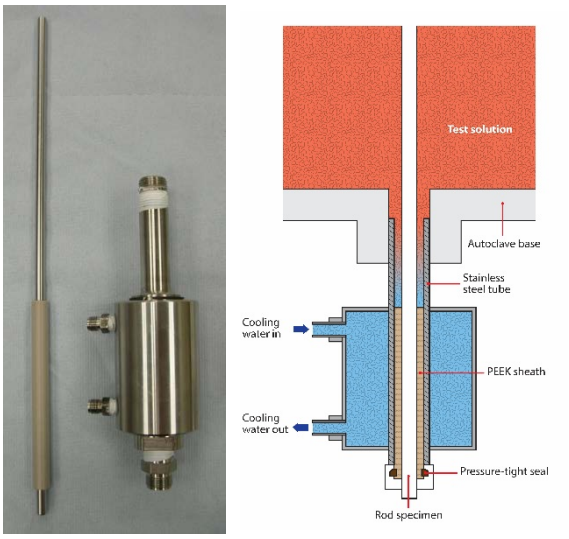

Figure 3: Photograph of polarisation specimen including water-cooled jacket (left), and schematic of their configuration in relation to the autoclave (right). The material shown in the image is for a S13Cr SS but the same configuration was used for the 316L SS.

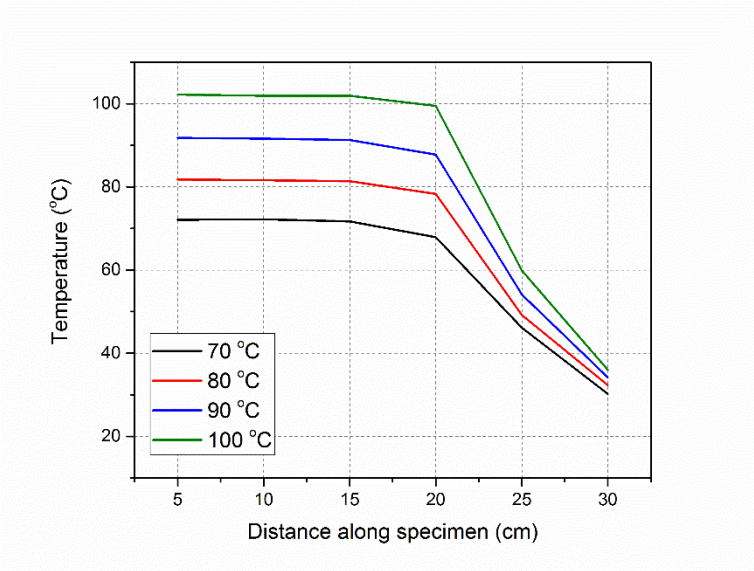

Figure 4: Temperature distribution measured along polarisation specimen from top to bottom at different autoclave temperatures.

3.1.3 Method for pitting and repassivation tests

Test solutions were prepared to represent produced water with a chloride concentration of 50,000 ppm, at a temperature of 110 °C. The solutions were buffered to a nominal pH (pH_{nom}) of either 4.0 or 4.5 under a standard set of conditions (1 bar CO_2, ambient temperature) by addition of CH_3COONa + HCl,

or $NaHCO_3$, respectively. The exact test conditions are given in Table 2 and are the same as those for the coupon tests described in Part 1[2]

A standard three-electrode configuration was used for the electrochemical measurements, with the specimen acting as the working electrode, the Hastelloy autoclave as the counter electrode and a high-pressure silver/silver chloride (Ag/AgCl, 3 M KCl) reference electrode. The reference electrode was maintained at room temperature during the tests by the use of a long salt bridge. After at least 1 hour, and once a quasi-steady open circuit potential (OCP) value had been reached (drift < 0.1 mV/min), the potential was stepped to -50 mV_{OCP} and then scanned in a positive direction at a scan rate of 10 mV/min. The scan was reversed when the current density reached 5 mA/cm^2 and then swept back to the initial value of the potential. Duplicate test specimens were used in each test.

Table 2: Test conditions for the potentiodynamic pitting and repassivation tests.

pH_2S (bar)	**pCO_2 (bar)**	**pH_{nom} 4.5**		**pH_{nom} 4.0**		**$[Cl^-]$ (ppm)**	**T (°C)**
		In situ pH	$[H_2S_{(aq)}]$* (ppm)	In situ pH	$[H_2S_{(aq)}]$* (ppm)		
0.0	1.000	-	-	3.92	0	50000	110
0.001	0.999	-	-	3.92	0.02		
0.010	0.990	4.93	0.22	3.91	0.22		
0.050	0.950	4.90	1.19	3.91	1.10		
0.100	0.900	4.87	2.36	3.91	2.21		
0.250	0.750	-	-	3.90	5.52		
0.010**	1.000	4.94	0	3.92	0		
0.100**	1.000	4.94	0	3.92	0		

** calculated from MTDATA (Hampton Thermodynamics Ltd) and previous thermodynamic data*
*** H_2S was introduced for 24 hours then removed by sparging with pure CO_2 before polarisation*

The procedure for achieving the desired test conditions within the autoclave (configuration shown in Figure 5) was as follows:

1. Test specimens were degreased in acetone, rinsed in isopropanol and dried in air.
2. The specimens were fitted into cooling coils and attached to the base of the autoclave, see Figure 3.
3. Test solution in a separate vessel was deaerated using high-purity nitrogen (> 99.998%) to reduce the dissolved oxygen concentration to less than 10 ppb according to a previously validated procedure[3]. The flow of nitrogen was used to simultaneously deaerate the autoclave containing the test specimens.
4. The deaerated solution was introduced to the deaerated autoclave using nitrogen pressure, following which the solution was sparged with nitrogen for a further hour to mitigate against oxygen ingress that may have occurred during transfer of the solution between vessels.
5. The solution was then sparged with a certified mixture of CO_2 and H_2S at the desired H_2S/CO_2 partial pressures at a rate of 100 ml/min for a minimum of 1 hour per litre of test solution.
6. Autoclaves were heated, with the gas mixture still flowing, to a temperature of 57 °C, at which point the gas flow through the submerged inlet was stopped.
7. The autoclave was then heated to 110 °C and the CO_2/H_2S gas mixture was flowed into the head space of the autoclave using an inlet tube above the level of the solution at 100 ml/min for 1 hour.
8. The inlet and outlet of the autoclave were sealed, and the test temperature was maintained to within ± 0.5 °C for the test duration.
9. The autoclave was vented and cooled back to ambient temperature, then purged with high-purity nitrogen for 24 hours before it was opened to remove the test specimens.

There was no applied stirring of the solution during these anodic polarisation tests.

Two additional tests were performed to decouple the effect of dissolved H_2S in solution and the effect of H_2S interaction with the passive film. For these tests, specimens were pre-exposed to the acetate-buffered pH_{nom} 4.0 test solution whilst saturated with $H_2S + CO_2$, after which electrochemical testing was performed in a purely CO_2 sparged solution. For these tests the above procedure was followed up to step 7, which was maintained for 24 hours instead of 1 hour. The solution was then cooled to 57 °C, to avoid tube blocking whilst sparging, and then sparged with pure CO_2 for 24 hours, after which the autoclave was sealed and heated to the test temperature as before.

As with the coupon tests, it was decided to fill and seal the autoclaves as opposed to charging them with gas continuously. This method is suitable when testing corrosion resistant alloys as the expected rate of consumption of H_2S is low and not anticipated to cause a significant depletion in these short-term tests. Achieving the final test pressure by heating the sealed autoclave is a convenient way of mitigating the risk of a salt blockage occurring in the inlet tube at higher temperature. However, when this is done with a mixture of two or more gases, the differential change in solubility of the gases can cause their relative partial pressures to change from that desired for the test. Step 7 is designed to prevent this by replenishing the headspace of the autoclave with the gas mixture in the correct stoichiometric ratio. If this is not done, then it is predicted, using MTDATA thermodynamic software, that the H_2S partial pressure could be up to 20%* greater than expected from its stoichiometric ratio in the gas mixture.

** calculated for a 50% full autoclave.*

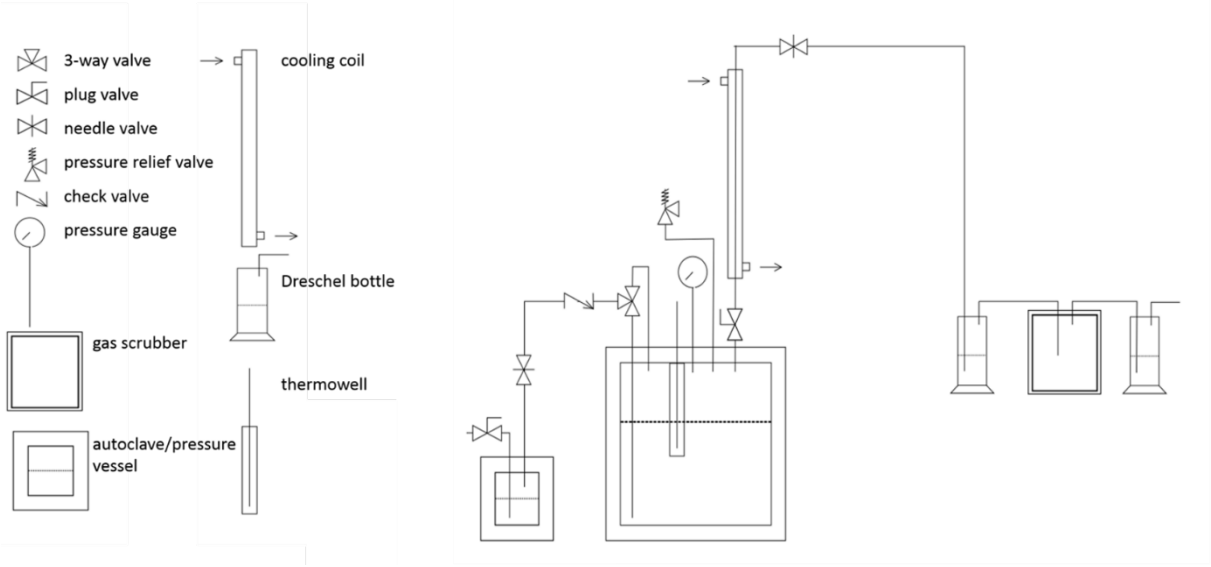

Figure 5: Autoclave configuration used for all tests at elevated temperature and pressure.

3.2 CATHODIC POLARISATION

3.2.1 Outline

A series of cathodic polarisation experiments was performed in an autoclave at elevated temperature and pressure. Due to the unavailability of a high-pressure, high-temperature rotating disk electrode, a custom-built specimen holder was used to enhance the mass-transport of species to and from the electrode surface. The specimen holder enables a magnetic stirrer to produce fluid shear across the specimen surface and was shown to significantly increase transport-limited current density during cathodic polarisation in the test environments, allowing activation-controlled conditions across a broader potential range. A diagram of the configuration of the specimen holder is shown in Figure 6. The specimen was hand-ground to a P1200 grit finish, $Ra < 0.1$ μm.

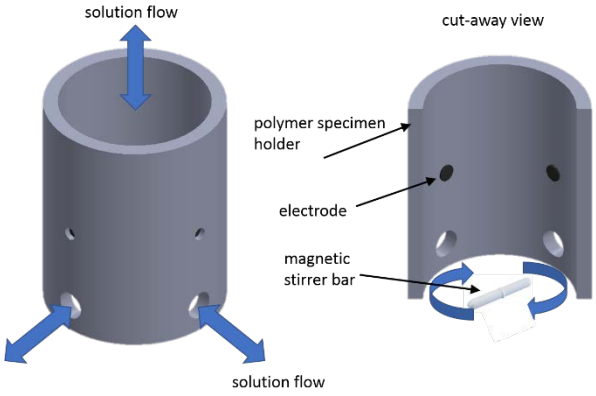

Figure 6: Diagram of the specimen holder used in cathodic polarisation autoclave tests (h = 80 mm, r = 32 mm).

3.2.2 Cathodic polarisation test specimens

The cathodic polarisation test specimens consisted of 5 mm diameter 316L SS disks (exposed area 0.196 cm^2) that were pressed into a tightly fitting polymer specimen holder. An electrical connection was made by spot welding a nickel wire, encapsulated within a PEEK jacket, to the back of each electrode and sealing the joint with epoxy resin.

3.2.3 Method for cathodic polarisation tests

The test conditions are listed in Table 3; buffering of the solution was achieved using CH_3COONa + HCl as previously described. These conditions were selected to determine the individual contribution of CO_2 and H_2S towards the cathodic current in the presence of a well-buffered brine. The autoclaves were deaerated and charged with CO_2/H_2S following the procedure in 3.1.3. A hotplate with a magnetic stirrer control was used to heat the autoclave and rotate the stirrer bar in the centre of the specimen holder. The stirrer speed was maintained constant throughout all tests. Specimens were then left to stabilise at OCP for at least 1 hour before polarising from OCP to -1 V_{OCP} at a rate of 10 mV/min. All tests were carried out in duplicate.

A second set of experiments was performed where specimens were left in the solution at OCP for 1 week prior to polarisation. This was done to determine whether the surface became a more effective catalyst for proton reduction through a longer duration of exposure to the H_2S-containing environment.

Table 3: Test conditions for the cathodic polarisation tests.

pH_2S (bar)	pCO_2 (bar)	pH_{nom} 4.0		$[Cl^-]$ (ppm)	T (°C)
		In situ pH	$[H_2S_{(aq)}]$* (ppm)		
0.0	0.0	3.92	0	50000	110
0.0	1.0	3.92	0		
0.01	0.99	3.91	0.22		
0.10	0.90	3.91	2.21		

** calculated from MTDATA and previous thermodynamic data*

3.3 ARTIFICIAL PIT EXPERIMENTS

3.3.1 Outline

A series of lead-in-pencil tests was performed to simulate the polarisation characteristics of a single corroding pit in the test environment. Lead-in-pencil electrodes are a convenient way of achieving this, as they comprise a thin wire embedded within an inert surrounding. As the electrode corrodes, it recedes into the inert support, enabling the development of a local chemistry that is separated from the bulk chemistry by a mass transport barrier. Limitations to this approach are that the electrode is essentially planar, and its surface area does not increase significantly as it is oxidised. This contrasts with a real pit, whose surface area increases with size and whose walls are electrochemically active.

Experiments were performed to establish the polarisation characteristics of the active surface in isolation from the passive surface. Further experiments were undertaken without applied polarisation to establish the extent to which coupling to a nominally passive macro-electrode can polarise a lead-in-pencil micro-electrode that has been activated by prior anodic polarisation, and to measure the magnitude of the coupling current between them.

3.3.2 Lead-in-pencil electrode specimens

Two types of lead-in-pencil electrode specimens were produced.

The first consisted of a short (~ 1 cm) length of 1 mm diameter 316L SS rod tightly encapsulated in a PEEK sheath. At one end, an electrical connection was made by spot welding a nickel wire encapsulated in PEEK and sealing the connection with a chemically resistant epoxy resin; the other end was wet ground to a P1200 finish using silicon carbide paper, giving an initial electrode surface area of 0.785 mm^2.

The second specimen consisted of a short (~ 1 cm) length of 50 µm diameter 316 L SS wire that was spot welded at one end to another short length (1 cm) of thicker nickel wire, with both wires encapsulated in PEEK tubing. Five lengths of the PEEK encapsulated wires were laid out in parallel and hot-mounted within a phenolic resin block. The mounting process applied high pressure to the liquid resin and forced it into the PEEK tube surrounding the thinner wire, forming a tight seal. The resin was broken away at the end containing the thicker nickel wire to allow an electrical connection to be made to an additional longer (30 cm) PEEK encapsulated nickel wire; all joints were sealed as previously described. As with the larger electrodes, the end containing the thin steel wire was wet ground to a P1200 finish using silicon carbide paper, giving an initial individual electrode surface area of 0.00196 mm^2.

A schematic of the two types of lead-in-pencil electrode specimen is shown in
Figure 7. The test specimen was flush with the surface. It is commonplace to fabricate lead-in-pencil electrodes by embedding wires in epoxy resin, which is a comparatively easy process. However, this was avoided since the very acidic local chemistry generated within the lead-in-pencil cavity left by the dissolution of the wire during oxidation can result in chemical attack on the epoxy and leaching of

organic compounds (confirmed by sampling and analysis), which may act as corrosion inhibitors and should therefore be avoided.

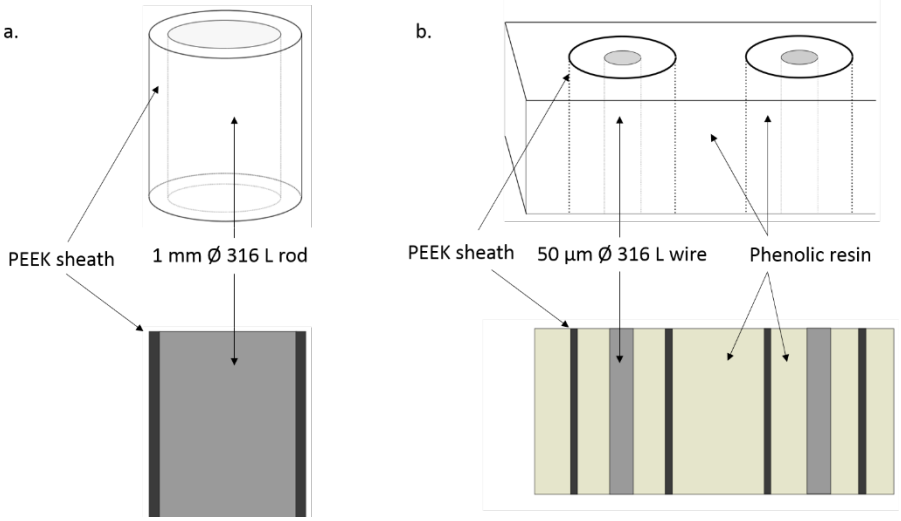

Figure 7: Schematic of the lead-in-pencil electrode specimens, in isometric projection (top) and cross-section (bottom).

3.3.3 Cyclic polarisation of lead-in-pencil electrode specimens

Both types of lead-in-pencil electrodes were tested in autoclaves which were prepared as described previously. Tests were conducted in simulated produced water environments at pH_{nom} 4.0, as summarised in Table 4. A three-electrode configuration was used for the electrochemical measurements, with the specimen acting as working electrode, the Hastelloy autoclave as the counter electrode and a high pressure silver/silver chloride (Ag/AgCl, 3 M KCl) reference electrode, which was maintained at room temperature during the tests by the use of a long salt bridge.

For both the 1 mm and the 50 µm diameter electrodes, cyclic polarisation was performed from -25 mV_{OCP} to 500 mV_{OCP} (OCPs were in the range -550 mV_{SCE} to -700 mV_{SCE}) at a rate of 10 mV/min in 0.01 bar and 0.10 bar of H_2S, to study the polarisation behaviour of the active surface. For the test performed in 0.01 bar H_2S, the micro-electrodes were coupled through a zero resistance ammeter (ZRA) to a coupon of the same material (exposed area 22.8 cm^2) upon completion of the potential sweep and repassivation of the wire. This enabled measurement of the galvanic coupling between the small surface and a large passive surface in the absence of externally applied polarisation.

A further test was performed on a fresh set of 50 µm diameter electrodes in which cyclic polarisation was performed over a small potential range from -680 mV_{SCE} to -480 mV_{SCE} (~ 0 mV_{OCP} to 200 mV_{OCP}) at a rate of 10 mV/min in the presence of 0.01 bar H_2S. As before, coupling between the micro-electrode and a coupon of the same material was performed after polarisation to observe the galvanic current. The rationale behind this procedure was that -680 mV_{SCE} was approximately the stable OCP of the micro-electrodes and -480 mV_{SCE} was approximately the OCP of the larger electrode. Hence polarisation from -680 mV to -480 mV would polarise the micro-electrode anodically without the potential being so high that unrepresentative very acidic pit chemistry might ensue should localised corrosion develop. The potential was then scanned back to the new OCP (~ -580 mV_{SCE}) of the microelectrode to ensure that when the two electrodes were coupled, the potential of the micro-electrode would be more negative than that of the coupon, thereby mitigating pit initiation on the coupon.

Table 4: Test conditions for the lead-in-pencil electrode polarisation tests.

pH_2S (bar)	pCO_2 (bar)	pH_{nom} 4.0		$[Cl^-]$ (ppm)	T (°C)
		In situ pH	$[H_2S_{(aq)}]$ (ppm)		
0.01	0.99	3.91	0.22	50,000	110
0.10	0.90	3.91	2.21		

** calculated from MTDATA and previous thermodynamic data*

4 RESULTS

4.1 PITTING AND REPASSIVATION

Polarisation data for the tests performed at pH_{nom} 4.0 in pure CO_2 are shown in Figure 8. The alloy exhibited a clear passive region and well-defined pitting potential, E_p, and repassivation potential, E_{rp}, values at around -200 mV_{SCE} and -300 mV_{SCE}, respectively. Here, the pitting potential is estimated from the onset of a sustained and significant increase in slope of the polarisation curve, while the repassivation potential is based on the potential at which the reverse polarisation curve crosses the forward polarisation curve. Good repeatability was observed between the duplicate tests.

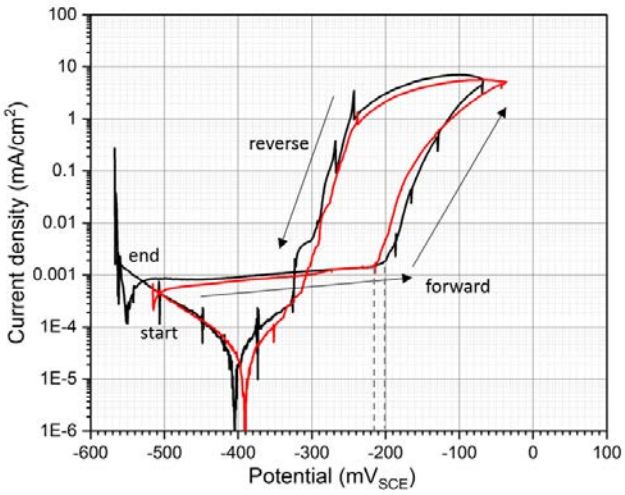

Figure 8: Plot of potentiodynamic polarisation at pH_{nom} 4.0, pure CO_2, 50,000 ppm Cl^- at 110 °C. The red and black lines represent test data for two different specimens.

Figures 9-12 show the polarisation data for the tests performed at pH_{nom} 4.0 and at H_2S partial pressures of 0.01 bar, 0.05 bar, 0.10 bar and 0.25 bar, respectively. The OCP in these tests showed little variation with H_2S concentration except for the more negative potential at 0.25 bar H_2S. However, the contrast between the polarisation curves obtained in the presence of CO_2 + H_2S compared with those in pure CO_2 is stark. While the cyclic polarisation curve in the presence of CO_2 shows a characteristic breakdown potential and repassivation potential, the behaviour in solutions containing H_2S indicates a more complex behaviour. Under just 0.01 bar H_2S, the passive region of the alloy was no longer observable, with the current density increasing initially from the OCP at an average rate of ~ 100 mV/decade, suggesting activation-controlled oxidation. Much lower anodic currents were apparent over the same potential range at the higher partial pressures of H_2S, which is not consistent with oxidation of H_2S as an explanation. Pitting corrosion at the OCP in the 0.01 bar H_2S test is the more likely process but that requires an explanation for the absence of a rapid rise in

current density with corrosion potential typical of pitting corrosion, and rationalisation of the initial lower current density upon anodic polarisation for 0.05 bar and 0.1 bar H_2S (see Discussion).

The additional anodic process of oxidation of H_2S, and uncertainty in the potential above which this becomes significant, makes it more challenging to identify clearly defined values of E_p in the polarisation curves., Nevertheless, the hysteresis in the polarisation curve upon reversal of the polarisation sweep indicates clearly that pitting has ensued. Here, the tests performed in 0.01 bar H_2S exhibited a repassivation potential more positive than the OCP, measured at around -375 mV_{SCE}, but at higher partial pressures the repassivation potential was below the initial OCP, demonstrating the impact of increasing H_2S partial pressure in inhibiting repassivation.

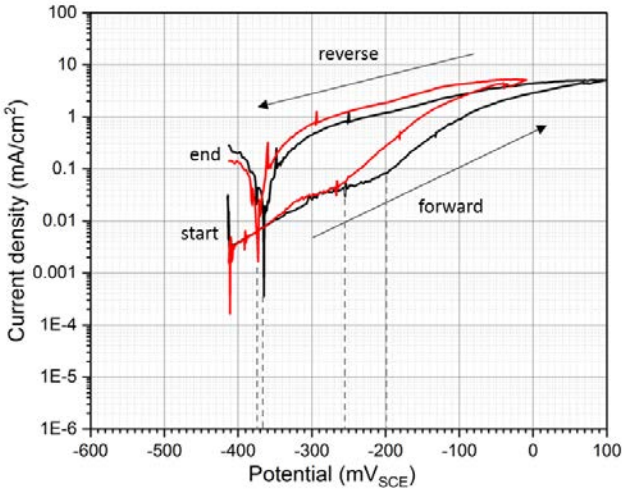

Figure 9: Plot of potentiodynamic polarisation at pH_{nom} 4.0, 0.01 bar H_2S, 50,000 ppm Cl^- at 110 °C.

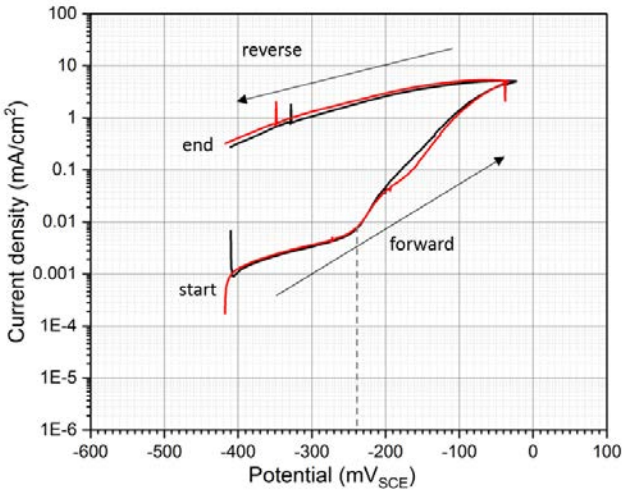

Figure 10: Plot of potentiodynamic polarisation at pH_{nom} 4.0, 0.05 bar H_2S, 50,000 ppm Cl^- at 110 °C.

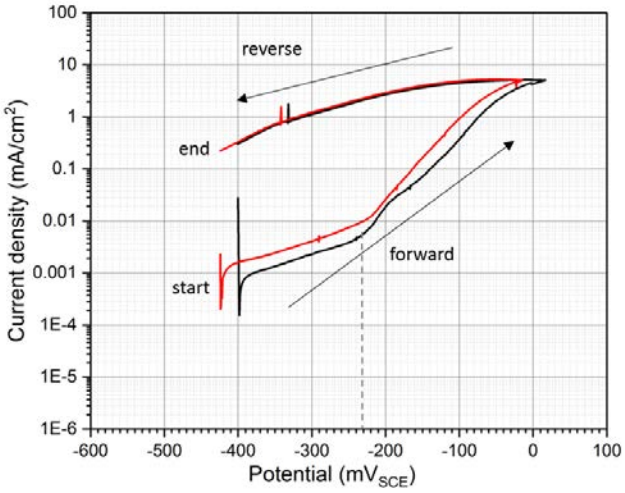

Figure 11: Plot of potentiodynamic polarisation at pH_{nom} 4.0, 0.10 bar H_2S, 50,000 ppm Cl^- at 110 °C.

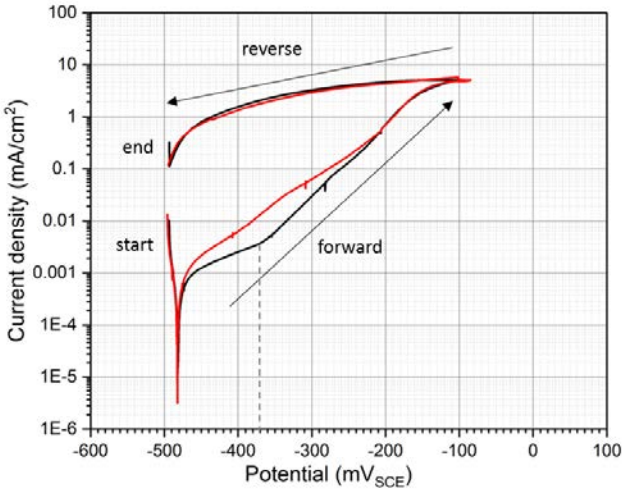

Figure 12: Plot of potentiodynamic polarisation at pH_{nom} 4.0, 0.25 bar H_2S, 50,000 ppm Cl^- at 110 °C.

Figures 13-15 show the polarisation data from the tests undertaken at pH_{nom} 4.5 in 0.01 bar, 0.05 bar and 0.10 bar of H_2S, respectively. A more negative OCP was observed in comparison to the tests at pH_{nom} 4.0, which would be expected owing to the lower H^+ concentration at the higher pH. In contrast to the tests at pH_{nom} 4.0, the data suggest a tendency for the OCP to shift in the positive direction as the partial pressure of H_2S increases, but this observation is tempered somewhat by the lack of repeatability in the data at 0.01 bar. The overall positive shift in OCP with increasing H_2S partial pressure, if interpreted as such, is hard to explain on the basis of a reduced anodic current density since that is not consistent with the anodic polarisation data. The cathodic polarisation data here are too limited to comment on enhanced cathodic reaction kinetics but by implication an increase is expected if a positive shift in OCP were to be explained. However, the in situ pH is scarcely changed with H_2S concentration (a maximum predicted variation of 0.06 units over the range of H_2S partial pressure tested) so either buffering is a factor, which would be surprising as the corrosion current at open circuit is modest, or there is an additional cathodic reaction. As evident in Figure 13 there is some variability in testing conditions, perhaps due to time of storage prior to testing, and too much interpretation would not be appropriate.

The anodic polarisation curves at pH_{nom} 4.5 had some similarities to those at pH_{nom} 4.0, although tending to show more clearly the inflections in the forward polarisation scan, indicating the possibility of more than one oxidation process. This transition was most distinguishable at the lowest H_2S partial pressure (0.01 bar). Perhaps the most notable difference was the trend of increasing anodic current density with increasing partial pressure of H_2S in the first 100 mV of polarisation from the OCP, which was not apparent for tests at pH 4.0. Similar to the tests at pH_{nom} 4.0, a repassivation potential more positive than the OCP was only observed for 0.01 bar H_2S, and for one test only (~ -400 mV_{SCE}).

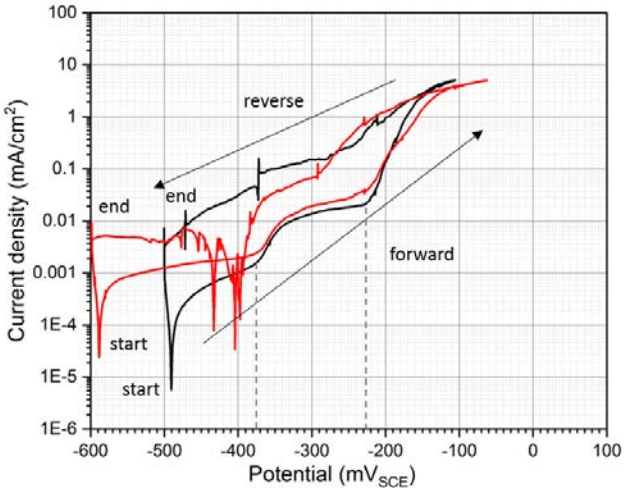

Figure 13: Plot of potentiodynamic polarisation at pH_{nom} 4.5, 0.01 bar H_2S, 50,000 ppm Cl^- at 110 °C.

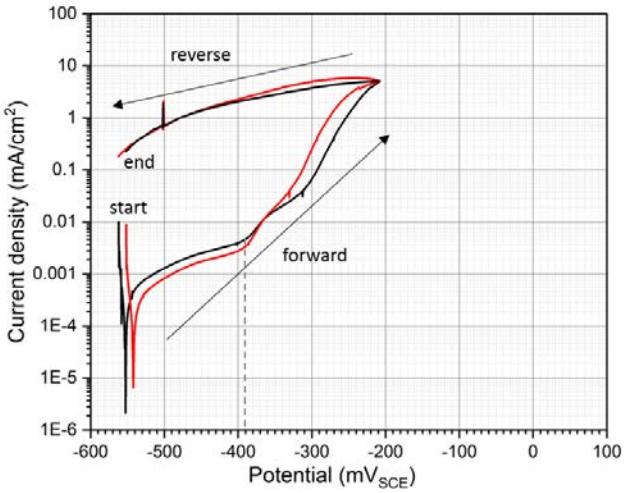

Figure 14: Plot of potentiodynamic polarisation at pH_{nom} 4.5, 0.05 bar H_2S, 50,000 ppm Cl^- at 110 °C.

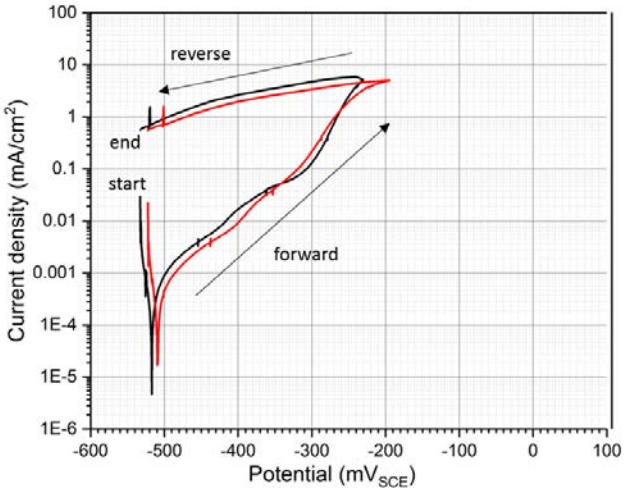

Figure 15: Plot of potentiodynamic polarisation at pH_{nom} 4.5, 0.10 bar H_2S, 50,000 ppm Cl^- at 110 °C.

Figure 16 and Figure 17 show the polarisation data at pH_{nom} 4.0 for the tests that were pre-exposed to 0.01 bar H_2S and 0.10 bar H_2S, respectively, for 24 h before cooling to 57 °C, sparging with CO_2, reheating to 110 °C and polarising in a purely CO_2 sparged solution. Comparing these results to those obtained from the tests performed in CO_2 without pre-exposure to H_2S (Figure 8), pre-exposure resulted in a substantial positive shift in OCP of up to 400 mV with respect to the OCP in pure CO_2. The magnitude of the shift was greater for the specimens that were pre-exposed at the higher H_2S partial pressure. Pre-exposure to H_2S shifted the OCP to potentials close to the E_p measured for pure CO_2 in the absence of pre-exposure. As a result, specimens that had been pre-exposed to H_2S did not exhibit the same broad passive regime in pure CO_2. However, interestingly, the anodic polarisation curves obtained for the pre-exposed specimens showed significantly more positive E_p and E_{rp} values than those in pure CO_2, which merits further investigation. Caution in drawing inferences from this work is necessary as the temperature was lowered to 57 °C and the solution sparged with CO_2 for 24 h before restoring to the test temperature.

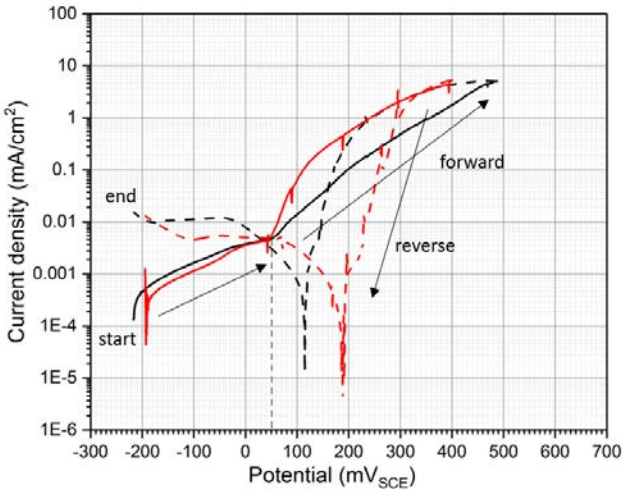

Figure 16: Plot of potentiodynamic polarisation at pH_{nom} 4.0, 1 bar CO_2 after pre-exposure to 0.01 bar H_2S, 50,000 ppm Cl^- at 110 °C (reverse scan is shown in dashes).

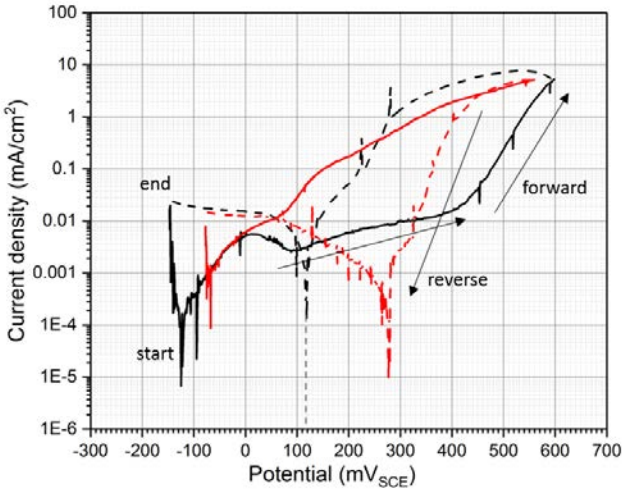

Figure 17: Plot of potentiodynamic polarisation at pH_{nom} 4.0 (measured under 1 bar CO_2 at ambient temperature), 1 bar CO_2 after pre-exposure to 0.10 bar H_2S, 50,000 ppm Cl^- at 110 °C (reverse scan is shown in dashes).

4.2 CATHODIC POLARISATION

The results of the cathodic polarisation tests performed in the presence of N_2, CO_2, 0.01 bar H_2S and 0.10 bar H_2S are shown in Figure 18. In the activation-controlled regime, between -500 mV_{SCE} and -700 mV_{SCE}, there was no significant influence of gas composition on the cathodic current, but there is evidently an additional cathodic current between the OCP and -500 mV_{SCE} in the 0.01 bar H_2S test. The latter suggests that an additional cathodic reaction has become observable. At more negative potentials, between -800 mV_{SCE} and -1000 mV_{SCE}, the cathodic current is controlled by mass transport and the influence of gas composition is evident. Pure CO_2 gives a higher limiting current than N_2, and addition of H_2S to the CO_2 increases the limiting current further. At polarisations greater than -1000 mV_{SCE}, water reduction becomes the dominant cathodic reaction. The OCP values at 0.1 bar H_2S were slightly more negative than measured in the anodic polarisation tests (cf. Figure 11). However, the test conditions were different, with significant stirring in the cathodic polarisation tests. There is no suggestion of transport control of the cathodic kinetics but there could be some subtle difference in the passive film formed at open circuit prior to polarisation. A more significant factor may be the different surface finishes, with machine-ground finish for the rods used in the anodic polarisation tests and the hand ground finish for the cathodic polarisation tests.

Figure 19 and Figure 20 show the effect on the cathodic polarisation of 7 days of pre-exposure to 0.01 bar and 0.10 bar H_2S, respectively. In 0.01 bar H_2S, there was a positive shift in OCP and an increase in the current measured at low polarisation compared with the other test environments. In addition, longer exposure led to an increased activation controlled current. In contrast, at 0.10 bar H_2S no significant effect of pre-exposure time was observed.

Owing to the unusual behaviour observed in the tests performed in 0.01 bar H_2S, a repeat test was undertaken, the results of which are shown in Figure 21. The repeat test did not exhibit the same current/potential behaviour as the original tests but did exhibit a similar OCP and a higher current under low polarisation than under any of the other test conditions. Considering the time dependence of the cathodic kinetics shown in Figure 19, it is not surprising that the tests exhibit low repeatability. To achieve repeatability in future, it may be beneficial to allow test specimens to equilibrate in the test environment for several days before performing measurements. The comparative insensitivity at

0.1 bar H_2S highlights a particular challenge in testing with H_2S and fully understanding its impact on electrochemistry.

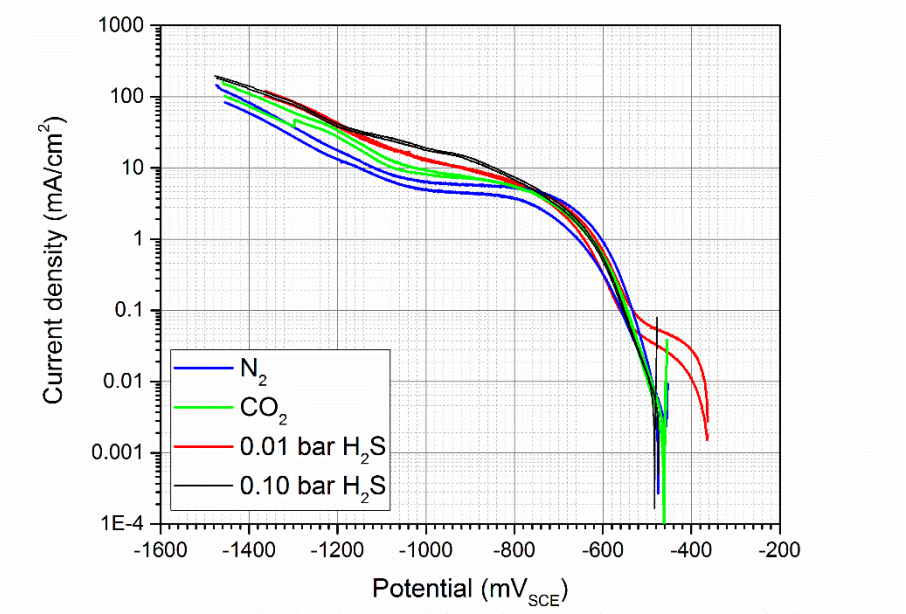

Figure 18: Comparison of cathodic polarisation measurements made in the presence of different gases in 50,000 ppm Cl^- at pH_{nom} 4.0 and 110°C.

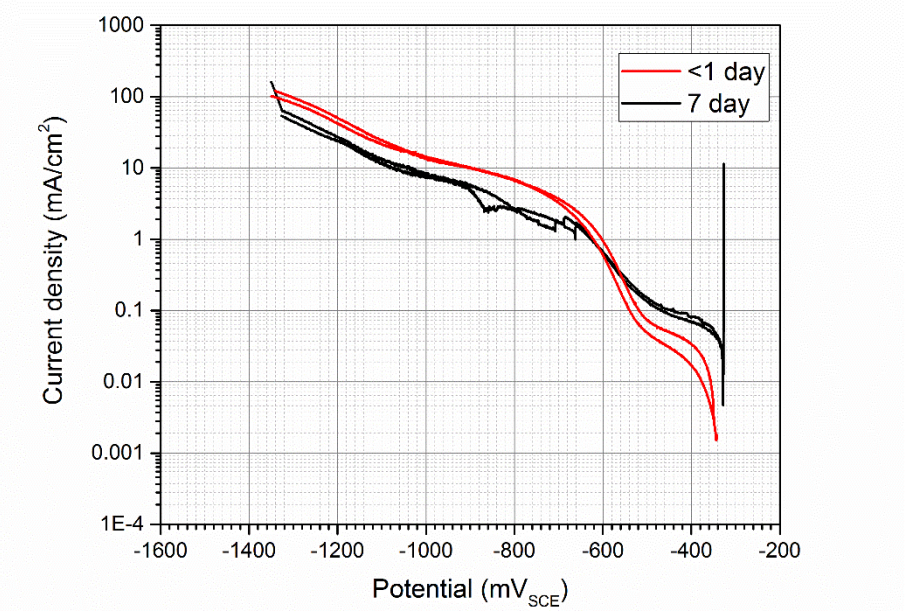

Figure 19: Comparison of cathodic polarisation measurements made after different lengths of exposure to 0.01 bar H_2S and 50,000 ppm Cl^- at pH_{nom} 4.0 and 110 °C.

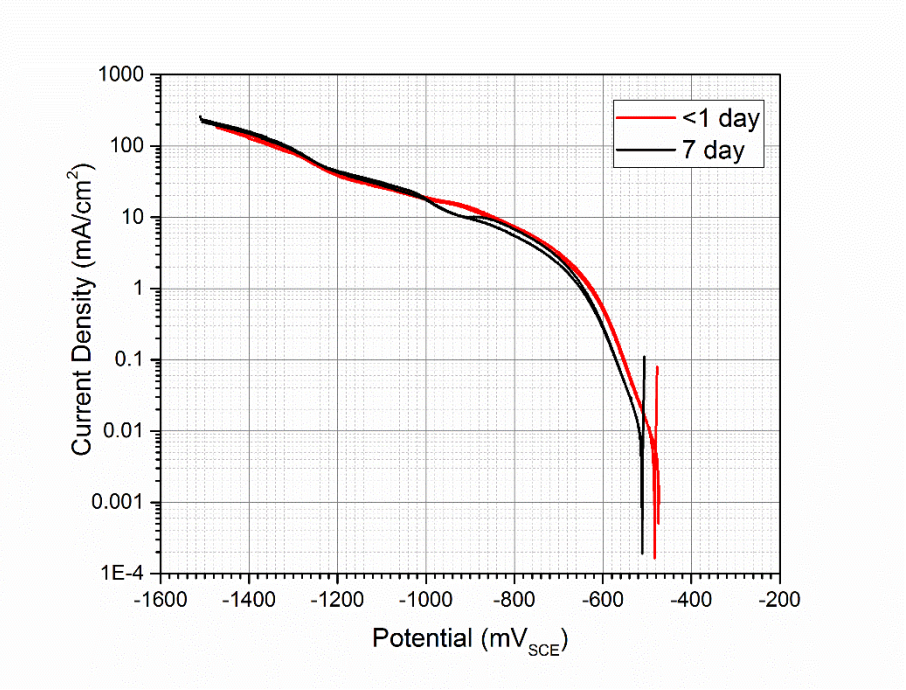

Figure 20: Comparison of cathodic polarisation measurements made after different lengths of exposure to 0.10 bar H_2S and 50,000 ppm Cl^- at pH_{nom} 4.0 and 110 °C.

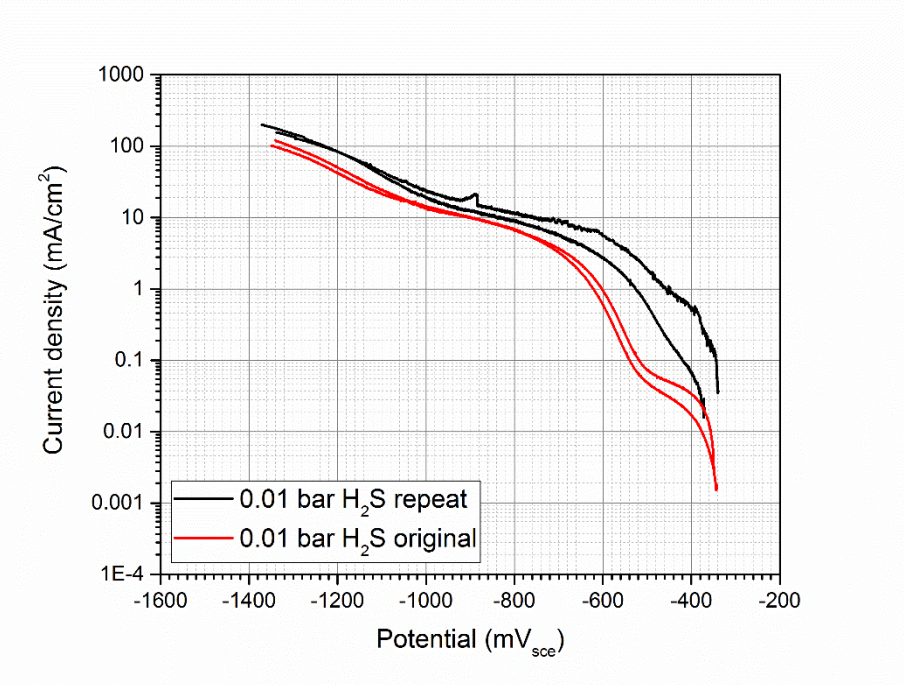

Figure 21: Comparison of cathodic polarisation measurements made in 0.01 bar and 50,000 ppm Cl^- at pH_{nom} 4.0 and 110°C.

4.3 ARTIFICIAL PIT EXPERIMENTS

4.3.1 Lead-in-pencil electrodes (1 mm diameter)

Figure 22 and Figure 23 show potentiodynamic polarisation plots for the 1 mm diameter lead-in-pencil electrodes tested at 0.01 bar and 0.10 bar H_2S, respectively. Compared with the large rod specimens in the anodic polarisation tests (Figure 12 and 14), the OCP was more negative (-550 mV_{SCE} to -600 mV_{SCE}) and the current densities were considerably higher, indicating activation of a greater proportion of the surface. Repeatability of the anodic polarisation curves was poor for 0.01 bar H_2S (despite repeatable OCP values) but good for 0.1 bar H_2S.

Increasing the H_2S partial pressure from 0.01 bar to 0.10 bar did not have a significant effect on the polarisation behaviour of the electrodes; in both environments there was a positive hysteresis of the polarisation curve and the repassivation potential was around -400 mV_{SCE}. At both H_2S concentrations, the hysteresis loop closed at potentials positive of the original OCP. On a large electrode this would typically indicate repassivation of corrosion pits on the surface (assuming that the whole surface was not activated); on such a small electrode this more likely indicates repassivation of a single pit or active surface.

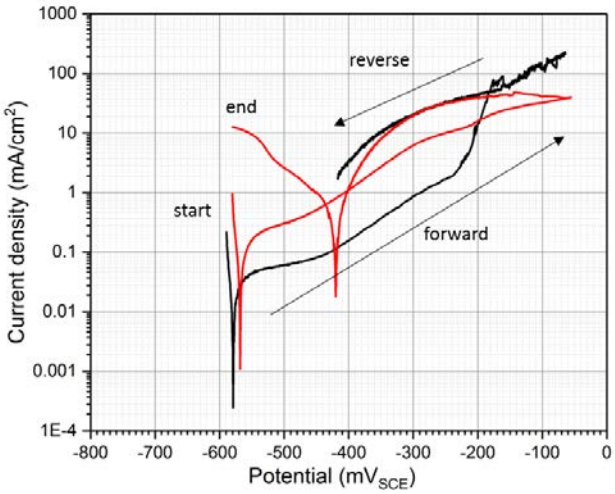

Figure 22: Potentiodynamic polarisation plot of 1 mm diameter lead-in-pencil electrodes at pH_{nom} 4.0, 0.01 bar H_2S, 50,000 ppm Cl^- at 110 °C.

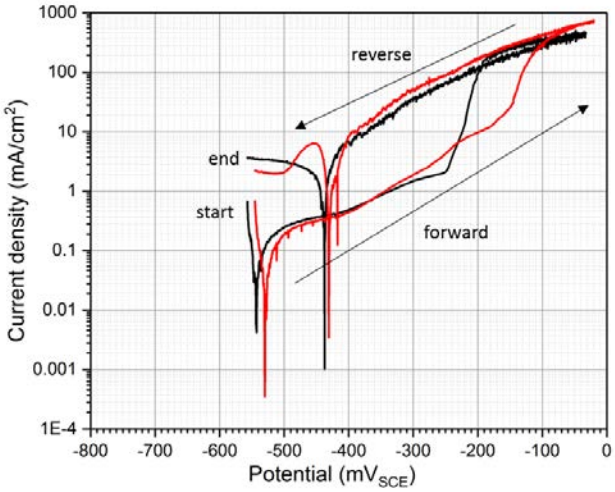

Figure 23: Potentiodynamic polarisation plot of 1 mm diameter lead-in-pencil electrodes at pH_{nom} 4.0 and 0.10 bar H_2S, 50,000 ppm Cl^- at 110 °C.

4.3.2 Lead-in-pencil electrodes (50 µm diameter)

Figure 24 and Figure 25 show potentiodynamic polarisation plots for the 50 µm diameter lead-in pencil electrodes over the range -25 mV_{OCP} to 500 mV_{OCP}. Compared with both the large rod electrodes and the 1 mm diameter lead-in pencil electrodes, the OCP of the 50 µm diameter electrodes was more negative, at around -600 mV_{SCE} to -700 mV_{SCE}. Under both 0.01 bar and 0.10 bar H_2S, small anodic polarisations of around 100 mV_{OCP} were enough to produce currents in the region of ~ 100 mA/cm^2, suggesting depassivation of the entire surface.

For tests performed in 0.01 bar H_2S, reversal of the scan direction led to negative hysteresis of the current sweep indicating reduced anodic activity. For the test performed at the higher concentration of 0.10 bar H_2S, the two identical electrodes showed different behaviour. One electrode performed as observed in the test at 0.01 bar H_2S, exhibiting negative hysteresis. The other showed a positive hysteresis and a considerable increase in current density to ~ 5 A/cm^2 upon reversing the scan direction, indicative of increased anodic activity and attributable to autocatalysis of the corrosion process.

Micro-electrodes were cyclically polarised, allowed to repassivate during the return sweep then galvanically coupled through a ZRA to a coupon of the same material. The coupled potential and galvanic current measured at 0.01 bar H_2S are shown in Figure 26. For both electrodes tested, the more noble coupon, whose OCP was ~ -480 mV_{SCE}, dominated the coupled potential, which resulted in anodic polarisation of the micro-electrode by around 200 mV. This resulted in a very high anodic current density at the microelectrode surface of 30-100 mA/cm^2, which is consistent with the data obtained from the cyclic polarisation measurements. When coupled to the coupon, one of the micro-electrodes exhibited a fairly constant galvanic current density of ~100 mA/cm^2 for close to 1 day. According to Faraday's law of electrolysis, this would be expected to recede the wire by approximately 3 mm. For this test, it is not clear why the galvanic current did not diminish over time; it is feasible that this reflects a quasi-steady condition where the dissolution is limited by a salt film formed on the recessed wire.

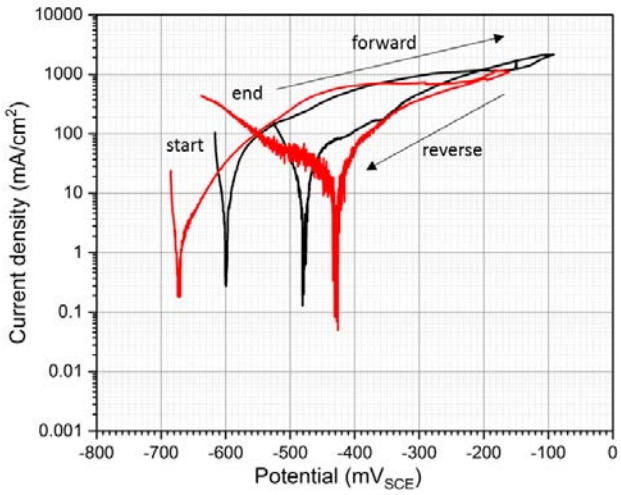

Figure 24: Potentiodynamic polarisation plot of 50 µm diameter lead-in-pencil electrodes at pH_{nom} 4.0, 0.01 bar H_2S, 50,000 ppm Cl^- at 110 °C.

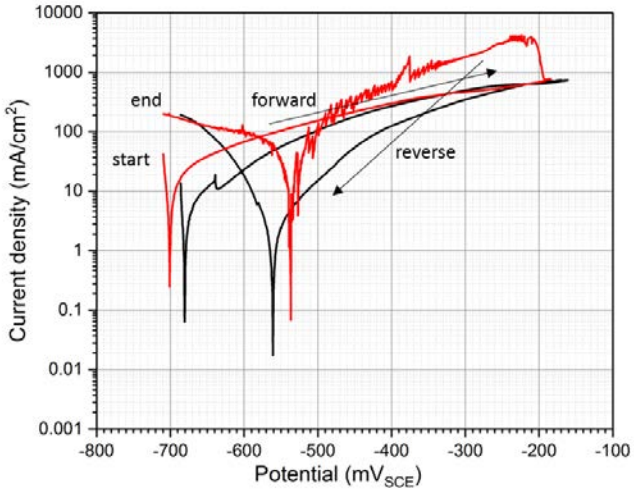

Figure 25: Potentiodynamic polarisation plot of 50 µm diameter lead-in-pencil electrodes at pH_{nom} 4.0, 0.10 bar H_2S, 50,000 ppm Cl^- at 110 °C.

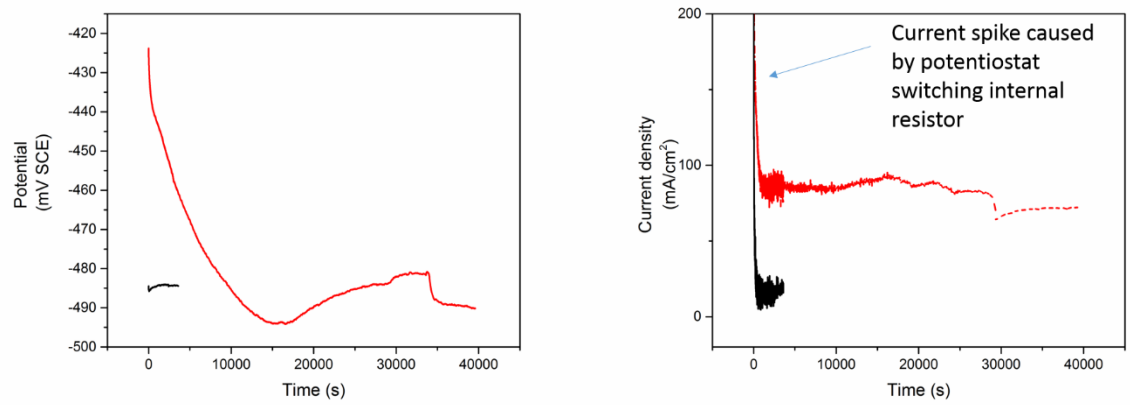

Figure 26: Coupled potential (left) and galvanic current (right) for the 50 µm diameter lead-in-pencil electrode and a corrosion coupon, following polarisation of the micro-electrode as shown in Figure 24. Test environment was 0.01 bar H_2S at pH_{nom} 4.0, 50,000 ppm Cl^- at 110 °C.

It should be noted that due to the high anodic polarisation performed prior to galvanic coupling, pit chemistry at the micro-electrode surface in this test was most likely a saturated metal salt solution with an extremely low pH owing to the hydrolysis of chromium ions. As such, this departs from the likely chemistry found in pits that form without externally applied polarisation, and so has limited relevance to the determination of likely propagation rates of pits that form in service conditions. To address this, a repeat test was performed where the maximum potential applied to the micro-electrode was set equal to the OCP of the passive surface in the same environment. As such, the ensuing pit chemistry that developed at the micro-electrode surface is considered to reflect that which may develop within a pit under open circuit conditions.

Over the reduced potential window, the cyclic voltammogram closely resembled that obtained under the higher potential window; after reaching the maximum applied potential of -480 mV_{SCE}, the reverse scan showed a negative hysteresis, indicative of a diminished anodic activity, which may be attributable to blocking of the surface by metal sulphide precipitates. When galvanic coupling was performed after polarisation, the trend was different to that observed for specimens that were polarised

to a more positive potential. Over a duration of about 17,000-18,000 s (~5 h), the galvanic current diminished substantially despite no significant change in the coupled potential. This may be attributed to either IR drop in the recess left by the corroded wire or blocking of the surface by precipitates. In this test, the galvanic current measured was still of the order of 100's of mA/cm^2, demonstrating that corrosion of the active surface will proceed rapidly even under a relatively small polarisation of ~200 mV; see Figure 27 and Figure 28.

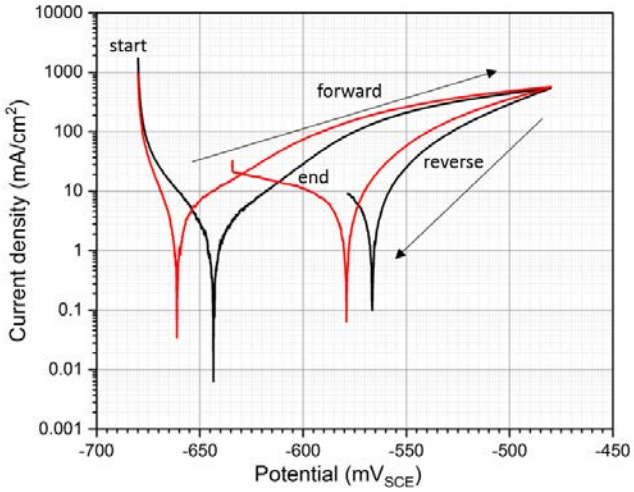

Figure 27: Potentiodynamic polarisation plot of 50 µm diameter lead-in-pencil electrodes at pH$_{nom}$ 4.0, 0.01 bar H_2S, 50,000 ppm Cl^- at 110 °C over a reduced potential scan range.

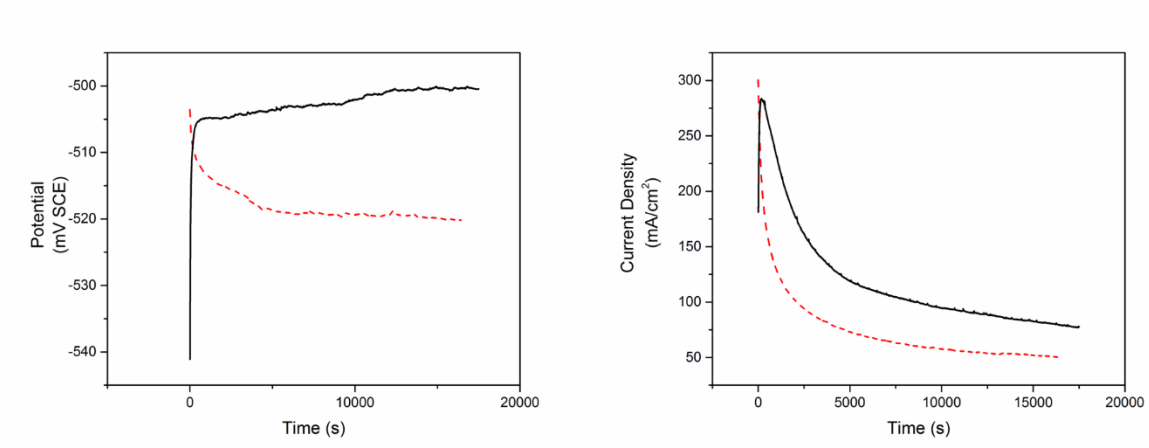

Figure 28: Coupled potential (left) and galvanic current (right) for the 50 µm diameter lead-in-pencil electrode and a corrosion coupon, following polarisation of the micro-electrode as shown in Figure 25. Test environment was 0.01 bar H_2S at pH$_{nom}$ 4.0, 50,000 ppm Cl^- at 110 °C.

5 DISCUSSION

5.1 PITTING AND REPASSIVATION TESTS

The results of the pitting and repassivation tests clearly showed that exposure to H_2S had a negative impact on the corrosion resistance of 316L SS. Previous studies on 316L SS have shown that, in the presence of H_2S, sulphur is integrated into the passive film diminishing its protectiveness[4-6], which has been ascribed to gradual sulphidisation of the oxide[4, 7]. Mott-Schottky analysis demonstrated that degradation of the oxide in the presence of H_2S is attributable to the change from a mixed n-type and p-type semiconductor to a purely n-type[4], which is more susceptible to attack by aggressive anions such as Cl^-. This is consistent with the observation of increased uptake of Cl^- into the passive film of 316L SS specimens exposed to H_2S in Part 1 of this study[2]. It has also been reported that in the presence of H_2S the degradation of the oxide film was greater at higher pH[6]. This observation was confirmed using both potentiodynamic polarisation and electrochemical impedance spectroscopy and was shown to arise from a reduction of chromium and an increase in sulphur species within the oxide layer[6]. This implies that HS^- could be more significant than H_2S in sulphidising the oxide, given that the extent of dissociation of H_2S in solution is greater at a higher pH. The results of the tests in which specimens were pre-exposed to H_2S before polarising in CO_2 suggests that sulphidisation of the oxide layer takes longer to reverse or may even be irreversible. However, it is not yet clear why this led to such a large positive shift in OCP. Noting the lack of a similar effect in the cathodic polarisation test results the indication is that this may have been influenced by the cooling/heating cycle that was required to replace the sour gas mixture with pure CO_2.

The anodic polarisation results in the forward scan do not show a consistent pattern of behaviour with respect to the effect of H_2S partial pressure. The complexity can be attributed to the interplay between applied potential, local pH in pits, bulk solution buffering capacity, H_2S concentration in solution, and possible oxidation of H_2S itself. In our previous coupon corrosion study[2], we showed that the greatest pit sizes and densities were observed at intermediate partial pressures of H_2S, specifically 0.01 bar, and at higher partial pressures, pitting was less extensive. This was explained on the basis of the inhibition of pit propagation by blocking of the pit surface by metal sulphide precipitation, which increased with increasing H_2S. Simple model calculations showed that solubility of metal sulphides increased with decreasing pH of the pit solution because of reduced tendency to precipitate. Using this understanding, we propose that at 0.01 bar H_2S, bulk pH_{nom} 4.0, pitting is initiated at the OCP and propagates, but the pit growth rate is constrained initially by porous metal sulphides, while the pH remains quite well buffered close to the OCP. Thus, a relatively weak dependence of current on potential is observed initially until continued anodic polarisation is sufficient to promote a more acidic pH in the pit, rendering the sulphides more soluble and correspondingly generating a greater pit current density. At higher partial pressures of H_2S, sulphide precipitation is relatively more dominant so that while metastable pitting may occur at the OCP the solution is well buffered by acetate ions and further development of the pit is suppressed. However, with increasing anodic polarisation the same process of local acidification in embryonic pits evolves despite the buffering, and significant pit development ensues. The polarisation scan was then reversed at a relatively high anodic potential, which would correspond with a highly acidic pit chemistry. In this case, the metal sulphides in the pit would be highly soluble, and the acidic conditions are sustained in a feedback process by a higher active corrosion current density, despite scan reversal, such that a greater suppression of the potential is required in order to repassivate.

The forward polarisation scans in the pH_{nom} 4.5 solution initiated at a more negative corrosion potential compared to test in pH_{nom} 4.0 and this led to an additional wave in the polarisation curve at low H_2S partial pressures (0.01 bar and 0.05 bar) that was not evident in the pH_{nom} 4.0 solution. The origin of this oxidation process is less clear but could simply reflect the passive current density, which is not markedly greater than that determined in CO_2, albeit the profile is not as flat. At potentials positive of the OCP in the pH 4.0 solution, the curves were not substantially different as a function of H_2S partial pressure. However, at a H_2S partial pressure of 0.1 bar, the forward scan in pH_{nom} 4.5 is quite different from that at lower partial pressures, with the current increasing more rapidly with

potential and the inflections almost smoothed out. It is possible that the reduced buffering capacity of the pH_{nom} 4.5 solution is enabling local acidification in embryonic pits, despite the lower potential and this provides sufficient solubility of metal sulphides to enable progressive pit development. The repassivation behaviour at pH_{nom} 4.5 reflects that of pH 4.0 and is explained on the same basis.

A fuller interpretation of the anodic polarisation curves depends on gaining knowledge on the oxidation of H_2S for these exposure conditions. Further work is planned with a more pitting resistant alloy that would give insight with respect to the oxidation of H_2S. Complementing that proposal, potential-hold experiments combined with post-mortem examination of the specimens could also identify the onset of pitting.

The inhibition of pit repassivation in these H_2S containing environments is consistent with previous findings[8] and supports the mechanism proposed by Marcus [9] and by Mat and Newman[10] whereby the sulphur species is considered to adsorb onto the active surface, preventing oxide formation.

Interpretation of these results in the context of the in-service performance of 316L SS is more difficult. In pits generated under a high anodic potential, the solubility of metal sulphides is much greater than for pits that form under open circuit, due to the highly acidic pH expected in the former. This may explain why the polarisation data did not fully reproduce the trend in environmental severity as observed in the coupon exposure tests in Part 1[2], where pitting was inhibited at the highest H_2S partial pressures. Improved correlation is expected with a more constrained potential window during the forward polarisation scan, polarising the sample just sufficiently to initiate pitting.

5.2 CATHODIC POLARISATION TESTS

The results obtained from the cathodic polarisation tests agree to an extent with the findings of both Kahyarian et al.[11] and Tribollet et al.[12], who observed that additions of H_2S did not influence the cathodic current density in the activation controlled regime but did increase the mass transport limited current. Tribollet et al.[12] ascribed the observation of a ‘second wave’ in the potential vs current plot to indicate the presence of direct H_2S reduction. If direct H_2S reduction made a significant contribution to the cathodic current, then the activation-controlled region of a potential vs current plot would be expected to show a H_2S concentration dependence. In the work of Tribollet et al.[12] a concentration dependence was observed at pH 6 but not at pH 4, which may suggest there is a small contribution from direct H_2S reduction towards near neutral conditions. At more acidic pH values H^+ reduction is expected to dominate. Kahyarian et al.[11] demonstrated that the presence of a second electrochemical wave can be reproduced numerically without the need for an additional cathodic reaction and can arise due to the buffering effect alone. However, as noted below, the buffering impact of H_2S is predicted to be negligible in the pHnom = 4.0 solutions (containing acetate), so this may not apply to the present situations.

The implication is that H_2S should only enhance the cathodic kinetics when the reaction is transport limited, and even then the magnitude of its effect is dependent on the presence of other buffers in the system (acetate was present in the tests at pH_{nom} 4.0). For a well-buffered system, the buffering capacity of the solution is negligibly increased by the presence of dissolved H_2S. The cathodic kinetics at the passive surface are under activation control in the potential range of the OCP in anoxic sour environments; hence the H_2S is expected to have no impact on the cathodic reaction. This is significant in describing the impact of H_2S on pitting corrosion in well-buffered solutions at open circuit, and points towards a predominantly chemical effect of H_2S as opposed to an electrochemical one.

However, it is perhaps a reflection of the complexity of the impact of H_2S on passive film properties that the electrochemical behaviour of H_2S, in being perceived to be acting solely as a buffer (in the absence of other more dominant buffers), is not consistent with the repeatable data obtained at 0.01 bar H_2S, where a clearly discerned increase in cathodic current density near the OCP was apparent, together with a shift in OCP to less negative potentials. For this case, extended pre-exposure led to an increased cathodic current density. The latter might suggest the development of a more catalytically

active surface film. However, there is a lack of consensus on the catalytic activity of iron sulphides[13,14,] which may reflect the different forms of the sulphide and range of condition in which investigation were undertaken. An alternative explanation for the increased current density is reduction of the metal sulphide film, noting the reduction of pyrrhotite to troilite reported by Esmaeely and Nesic[14]. However, this explanation would have envisaged that during 1 h pre-exposure of this 316L SS, significant sulphide was formed and then reduced upon cathodic polarisation. It is reported elsewhere[15] that mackinawite is formed first (over a day) in corrosion of carbon steel in H_2S at temperatures close to the present testing condition and there is no evidence for reduction of mackinawite. Nevertheless, the possibility of sulphide reduction cannot be ruled out entirely. Unfortunately, the vast majority of investigations on the electrochemical nature of metal sulphides have been for carbon and low alloy steels with less focus on corrosion resistant alloys.

From a more practical perspective. the influence of exposure time on the cathodic current measured at pH_{nom} 4.0, 0.01 bar H_2S suggests that a longer equilibration period may be required to obtain repeatable results. This challenges the relevance of using polarisation data obtained after just 1 h of exposure to characterise environments in which materials are exposed for considerably longer durations.

5.3 LEAD-IN-PENCIL TESTS

Lead-in-pencil electrodes were used to give insight into the polarisation behaviour of the active surface in isolation. When large area electrodes are used, local depassivation takes the form of pits, which results in an unknown ratio of active surface to passive surface; hence, the nominal current density is not representative. For the lead-in-pencil electrodes the measured current densities were considerably higher than those obtained for the large area electrodes, demonstrating that a greater proportion of the surface had become active. For the 50 µm diameter electrodes, it is assumed that the entire surface becomes active and the current density reflects that of the active surface within a corroding pit.

It was also observed that the smaller electrodes tended to have a more negative OCP, suggesting a higher rate of dissolution; see Table 5. Increased dissolution of the smaller electrodes could be attributed to crevice corrosion at the interface of the metal and the insulating material; for smaller electrodes the crevice accounts for a greater proportion of the total area.

Table 5: Variation of average current density with electrode size during anodic polarisation.

	50 µm diameter electrode	1 mm diameter electrode	Large area electrode
Current density at ΔE = +100 mV (mA/cm^2)	10 – 100	0.1 – 10	0.001 – 0.01
% activation of surface (assumed)	100	~ 10	~ 0.1
OCP (mV_{SCE}) (pH_{nom} 4.0)	-740 – -610	-580 – -530	-480 – -400

Measurements of the coupled potential of a large area coupon and the 50 µm diameter electrodes show that the coupled potential ranged from -520 mV_{SCE} to -480 mV_{SCE}, which was very close to the open circuit potential of the coupon. This means that when coupled together, the coupon undergoes only a very slight cathodic polarisation and the micro-electrode undergoes a substantial (~ +200 mV) anodic polarisation, as described in Part 1 of this study[2]. There are several implications to this, as follows:

1. The total anodic current within the pit must be small relative to the total passive current at the specimen surface. A simple calculation using a pit current density of 0.1 A/cm^2 and a pit of

30 μm depth yields a total current of about 6 μA, which is small compared to the total passive current at these temperatures.

2. Accordingly, formation of a single, or possibly several, pits will not cause a large potential drop in this test system and multiple pits can coexist. This contrasts with aerated solutions at ambient temperatures, for which the passive current density is very low, and where formation of a single pit is sufficient to depress the mixed potential.
3. The pit is likely to generate a slightly acidified chemistry relative to the bulk solution, which in the presence of H_2S inhibits repassivation. The anodic current density in an active small diameter lead-in-pencil pit was measured to be in the region of 10-100 mA/cm^2. The time-averaged current density required to produce a pit of given size can be derived from equation 1 and is plotted as a function of pit growth duration in Figure 29.

$$v = \frac{ItM}{\rho FZ} \quad (1)$$

Where,

- v is the volume of the of a hemispherical pit (cm^3)
- ρ is the density of the corroding surface taken as 7.8 g/cm^3
- t is the time for which the current flows (s)
- I is the total anodic current flowing in the pit (mA)
- F = 96485 C mol^{-1} is the Faraday constant
- M is the molar mass of the substance taken as 55.845 g mol^{-1}
- z is the valency number of ions of the substance, taken as 2 electrons transferred per ion

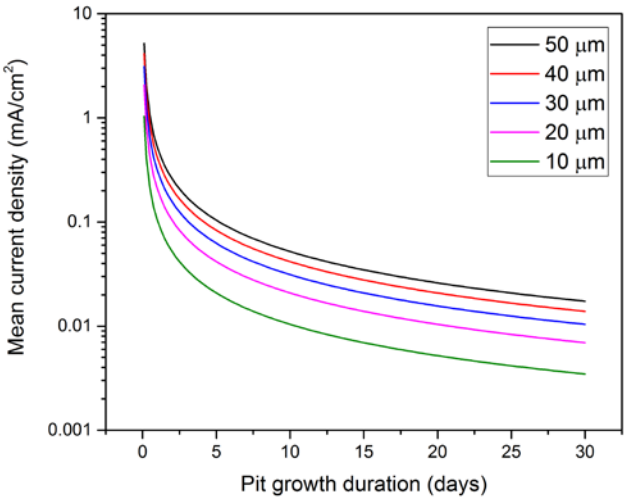

Figure 29: Plot of mean current density vs pit growth duration for different depths of hemispherical pit (calculated from Equation 1).

Thus, for a pit of depth of 50 μm measured after 30 days exposure, the time-averaged current density to achieve this depth would be just slightly greater than 0.02 mA/cm^2. In 30-day coupon tests[2], very few pits attained this depth. Relative to the active corrosion rate measured in the lead-in-pencil pit, which would generate this depth in less than a day, the observations from the coupon test would suggest that most pits examined ex situ had either died or had slowed substantially in growth rate. An inverse dependence of pit growth rate on pit depth (and correspondingly elapsed time) is normal. However, if the currents from lead-in pencil pits were applicable to real pits the growth rate would have to decrease dramatically with depth. The minimum pit current density required in H_2S containing solution to sustain an active pit at different pit sizes is less clear. Unfortunately, tests involving

coupons exposed for different exposure time to estimate the time-dependence of pit growth rate were not conclusive.

5.4 MECHANISTIC INSIGHTS

Overall, the results support the idea that H_2S enables pitting to take place at relatively low potentials, via chemical reaction with the passive film that makes it more vulnerable to attack by chloride as discussed in Part 1[2] which may explain also why H_2S can increase the depassivation pH of stainless steels[16,17]. Once a pit has initiated due to the defective passive film, the active surface may experience an anodic polarisation by the passive surface of up to 200 mV. This polarisation of the active surface will result in an imbalance between the local anodic and cathodic current densities, which will lead to slight acidification of the pit. If this is sufficient to inhibit repassivation (pH 3-5 depending on the grade of steel and H_2S level[14,15]) the pit will continue to propagate. The propagation rate will be rapid owing to the high potential dependence of the current density at the active surface. If unconstrained by transport limitations, pits would be projected to grow with current densities of 10-100 mA/cm^2, meaning a depth of 100 µm could be achieved in just a few hours (Figure 29), which suggests that pits either have a very short lifetime, or transition to a regime of substantially reduced growth rate.

6 CONCLUSIONS

- Repassivation potentials for 316L SS derived from anodic polarisation tests with different partial pressures of H_2S in simulated oilfield environments do not reflect the behaviour in coupon exposure tests and were evidently measured under overly severe conditions. The very acidic pit environment generated at high anodic potentials is considered to artificially maintain free H_2S in the pit (resulting in deeper pits and a more negative repassivation potential) by enhancing the solubility of metal sulphide that would otherwise precipitate and block pit propagation under freely corroding conditions.
- Cathodic polarisation curves in 0.1 bar H_2S showed little difference from tests in 1 bar CO_2 saturated solution without H_2S, especially in the activation-controlled regime present at the current densities practically relevant to the passive surface surrounding an active pit. However, this was not consistent with the repeatable data obtained at 0.01 bar H_2S, where a clearly discerned increase in cathodic current density near the OCP attributable to H_2S was apparent, together with a shift in OCP to less negative potentials. For this case, pre-exposure increased the current density near to the OCP. This enhancement could reflect a catalytic effect associated with a modified passive film or another reduction process, perhaps reduction of metal sulphides.
- Lead-in-pencil pit studies suggested that current densities density at the active surface could be of the order of 10-100 mA/cm^2. This would imply rapid pit growth and suggests that most of the pits observed ex situ, following materials qualification testing, had already stopped growing significantly when the test was terminated.

7 ACKNOWLEDGEMENTS

This work was supported by the National Measurement System of the United Kingdom Department for Business, Energy, and Industrial Strategy.

8 REFERENCES

1. Hinds, G., Wickström, L., Mingard, K., Turnbull, A., Impact of surface condition on sulphide stress corrosion cracking of 316L stainless steel, Corrosion Science, 72, 43-52 (2013).
2. Hesketh J, Dickinson EJF, McMahon G, Turnbull A, Hinds G, Influence of H_2S on the localised corrosion of 316L stainless steel: Part 1 – Coupon testing, NPL Report MAT 92, 2020
3. Hesketh J, Cooling P, Hinds G, Validation of oxygen purge techniques for stress corrosion cracking tests, NPL Report MAT 71, 2015
4. Ding J, Zhang L, Lu M, Wang J, Wen Z, Hao W, The electrochemical behaviour of 316L austenitic stainless steel in Cl^- containing environment under different H_2S partial pressures, Applied Surface Science, 289, 33-41 (2014)
5. Wang Z, Zhang L, Tang X, Zhang Z, Lu M, The surface characterization and passive behavior of Type 316L stainless steel in H_2S-containing conditions, Applied Surface Science, 423, 457-464 (2017)
6. Wang Z, Zhang L, Zhang Z, Lu M, Combined effect of pH and H_2S on the structure of passive film formed on type 316L stainless steel, Applied Surface Science 458, 686-699 (2018)
7. Ravindranath K, Al-Wakaa B, Tanoli N, Shalaby HM, The effect of chloride-hydrogen sulfide synergism on the stress corrosion cracking susceptibility of type 321 stainless steel, Corrosion 73, 1268-1279 (2017)
8. Hinds G, Wickström L, Abda J, Turnbull A, Smith V, Woollam R, Novel method for determination of pitting susceptibility in aggressive environments at elevated temperature and pressure, Corrosion Science 85, 33-41 (2014)
9. Elbiache A, Marcus P, The role of molybdenum in the dissolution and the passivation of stainless steels with adsorbed sulphur, Corrosion Science 33, 261-269 (1992)
10. Mat S, Newman RC, Local chemistry aspects of hydrogen sulfide-assisted stress-corrosion cracking of stainless steels, NACE International, Houston, TX, 1994
11. Kahyarian A, Nesic S, H_2S corrosion of mild steel: A quantitative analysis of the mechanism of the cathodic reaction, Electrochimica Acta 297, 676-684 (2019)
12. Tribollet B, Kittel J, Meroufel A, Ropital F, Grosjean F, Sutter E, Corrosion mechanisms in aqueous solutions containing dissolved H_2S. Part 2: Model of the cathodic reactions on a 316L stainless steel rotating disc electrode, Electrochimica Acta 124, 46-51 (2014)
13 Heift D, Iron Sulfide Materials: Catalysts for electrochemical hydrogen evolution, Inorganics, 7 (2019) 75.
14. Esmaeely SN, Nesic S, Reduction reactions on iron sulfides in aqeous acidic solutions, J. Electrochem. Soc. 164, C664-C670 (2017)
15 Gao S, Brown B, Young D, Singer M, Formation of iron oxide and iron sulfide at high temperature and their effects on corrosion, Corros. Sci., 135, 167-176, 2018.
16. Azuma S, Tsuge H, Kudo T, Moroishi T, Crevice corrosion of duplex stainless steel in simulated sour gas environments, Corrosion 45, 235-242 (1989).
17. Azuma S, Kudo T, Crevice corrosion of corrosion-resistant alloys in simulated sour gas environments, Corrosion 47, 458-463 (1991)